Mineralogia, vol. 54, 2023, 89-104 *Original Paper*

DOI: 10.2478/mipo-2023-0010

Geological and Mineralogical Analysis of Phosphorites in the Jebel Dhyr Syncline, Eastern Algerian Atlas

Salim Boulemia[1,2], Riheb Hadji[3,4,7,*], Salah Bouhlal[5], Younes Hamed[6,7], Houda Besser[7], Kaouther Ncibi[7]

[1]Department of Earth Sciences and the Universe, Faculty of Exact Sciences and Natural and Life Sciences, Echahid Larbi Tebessi University, Tebessa, 12000, Algeria
[2]Laboratory of sedimentary Environment and hydric and minerals resources, Faculty of Exact Sciences and Natural and Life Sciences, Echahid Larbi Tebessi University, Tebessa, 12000, Algeria
[3]Department of Earth Sciences, Institute of Architecture and Earth Sciences, Farhat Abbas University, Setif, 19000, Algeria
[4]Laboratory of Applied Research in Engineering Geology, Geotechnics, Water Sciences, and Environment, Farhat Abbas University, Setif, 19000, Algeria
[5]Department of Earth Sciences, Faculty of Science, University of Tunis, Tunisia
[6]Department of Earth Sciences, Faculty of Sciences of Gafsa, university of Gafsa, Tunisia
[7]International Association of Water Resources in the Southern Mediterranean Basin, Tunisia

*Corresponding author: hadjirihab@yahoo.fr

Abstract

The characterization of phosphorite features within specific North African sedimentary series remains incomplete. Hence, the primary aim of this research is to determine the composition of powder patterns and phosphatic allochem fragments within the Jebel Dhyr syncline, situated in northeastern Algeria. By focusing on this region, the study endeavors to investigate the mineralogical properties and geochemical aspects of Paleocene-Eocene phosphorites in the broader context of North Africa. The methodology employed encompasses geological, petrographic, geochemical, and mineralogical analyses of the rocks. To achieve this objective, we have employed various techniques including thin section analysis, atomic absorption spectrometry, and X-ray diffraction (XRD). The geological section across the Jebel Dhyr area has revealed a succession of horizontally layered rocks. These rocks consist of eight prominent phosphorite layers interspersed with carbonate formations. Additionally, occasional thin layers of flint can be observed within these carbonate layers. XRD analysis of the whole rock established the presence of apatite group minerals such as hydroxylapatite, fluroapatite, francolite, and dahllite. Other minerals identified include carbonates, quartz, zeolites, feldspar, clays, sulphides, and gypsum. XRD recordings on the phosphatic allochem grains (pellets, coprolites, intraclasts, and shark teeth) identified different mineral phases, with coprolites and pellets showing hydroxylapatite and fluorapatite, sometimes associated with dahllite, while granules of different forms revealed hydroxylapatite associated with fluorapatite or francolite. Teeth from the Jebel Dhyr phosphate beam showed the systematic presence of fluorapatite. This study provides valuable information for the comprehensive utilization of phosphorus resources in the Algeria-Tunisia border.

Keywords: phosphorites, Paleocene-Eocene, Jebel Dhyr, XRD, apatite group

1. Introduction

The sustainability of modern human civilization depends heavily on the availability and management of Earth's natural resources (Kallel et al. 2017; Besser et al. 2021; Ncibi et al. 2021; Bagwan et al. 2023). Nearly every industry requires minerals as essential inputs for their operations (Zeqiri et al. 2019; Fredj et al. 2020; Kerbati et al. 2020; Zerzour et al. 2020, 2021). Valuable chemical elements and useful minerals can be found in rocks, soils, and water (Nekkoub et al. 2020; Benmarce et al. 2021; Orabi et al. 2023; Sankar et al. 2023). Phosphorite is a vital resource that is essential for agriculture, as it is a primary source of phosphorus for fertilizers (Gadri et al. 2015; Rais et al. 2017; Dahoua et al. 2018; Anis et al. 2019; Barra et al. 2019; Zhang et al. 2019).

Phosphorus (P) is an indispensable component of all living organisms, including plants and animals (Crosby, Bailey 2012). Due to their significance as agricultural fertilizers, phosphate minerals are widely utilized, thereby making their exploration, exploitation, and processing highly valuable (Barra et al. 2019; Boulemia et al. 2021). Sedimentary phosphates, which possess high concentrations of phosphorus, represent the most crucial mineable phosphate ores globally (Yi et al. 2013; Buccione et al. 2021). Phosphorite mineralization can be found in strata spanning from the Precambrian to the Holocene, but it appears to be particularly abundant from the late Cretaceous to the Eocene (Notholt 2005). The vast Tethyan phosphogenic province, which stretches from Morocco in the west to Iraq and Turkey in the east, is particularly noteworthy, as it is estimated to hold approximately 70% of the world's phosphorite reserves (Abed et al. 2005; Garnit et al. 2017; Hamed et al. 2017, 2018; El Bamiki et al. 2021; Zhang et al. 2021).

Phosphorite is a marine sedimentary non-detrital deposit containing at least 18 wt% of P_2O_5 (Gál et al. 2020). The authigenic phosphatic particles in sedimentary rocks are present as concretions (pellets, nodules and crusts), composed mainly of apatite group minerals typically in cryptocrystalline masses (grain sizes < 1 μm) referred to as 'collophane'. They are hosted in calcareous or siliceous groundmass, commonly with brownish, yellowish or whitish colour (Boulemia et al. 2015).

The classification of the apatite group minerals is based on the presence of chloride, fluoride, carbonate, hydroxyl, and oxygen anions. The most abundant pure stoichiometric apatite are fluorapatite $Ca_5(PO_4)_3F$, hydroxylapatite $Ca_5(PO_4)_3(OH)$ and chlorapatite $Ca_5(PO_4)_3Cl$ (Fleet, Liu 2005) however 'carbonate-apatite' $Ca_5(PO_4,CO_3)_3(OH,F)$ is the main phosphate mineral (Sengul et al. 2006). Generally, the hexagonal crystal size of this apatite is about a few microns (Dar et al. 2017). Silica, clayey and calcareous materials constitute the gangue matrix for phosphates of sedimentary origin. The most sedimentary calcareous phosphate rocks have significant amounts of carbonates, and are considered as carbonate-apatite or francolite (Jaballi et al. 2019; Abou El-Anwar, Abd El Rahim 2022). To date, not a lot of studies on phosphorites have been undertaken in the transboundary Tebessa El Gasrine collapsed basin. We enumerate the bio-stratigraphic study of Flandrin (1948), the petro-mineralogical contribution of Boulemia et al. (2015), and the geochemical analyses of Kechiched et al. (2020) and Ferhaoui et al. (2022), which advances our contribution as the first research that deals with the qualitative analysis of the Jebel Dhyr syncline phosphorites. The questions asked are: Are the phosphorites of the Tebessa-Casserine collapsed basin mineralogically monotonous? Are they of the same family as those of North Africa? To answer these questions, our research focuses on the mineralogical characterization of the phosphate rocks of the Jebel Dhyr syncline. The outcome of the present work permits better elucidation of the mineralogy of the phosphorite rocks in order to recognize its detailed composition (bulk rock and phosphatic allochem grains) and contribute to deducing the diagenetic history and the depositional environment.

2. General Setting

2.1. Tectonics and Paleogeography

The study region belongs to the eastern edge of the Saharan Atlas on the Algerian and Tunisian border (Brahmi et al. 2021; Hamed et al. 2022a, b). It is 20 km of distance northeast of the chief province town of Tebessa (Fig. 1). Tebessa-El Kasserine basin is semi-arid, with low rainfall in most parts of the basin in winter and high temperatures in summer (Boubazine et al. 2022; Taib et al. 2023).

The Atlas tectonic phase structured a series of anticlines and synclines of NE-SW to ENE-WSW orientation. An extensive phase reactivated earlier faults, allowing the creation of a cross-border rift. These structures are pre-Miocene and would have started in the Campanian to reach their paroxysmal phase in the Lutetian. After the deposition of the continental lower Miocene, a resumption of tangential compressions is attested by shifts affecting these Eocene deposits. The filling of these ditches is made up of continental sediments attributed to the Plio-Villafranchian and the recent Quaternary (Fleury 1969). The morphology of the study area shows a wide syncline, alternated by narrow, coffered anticlines in axial directions (WNW-ESE). These structures are intersected by a few major transverse faults (Tamani et al. 2019; Hamad et al. 2018, 2022).

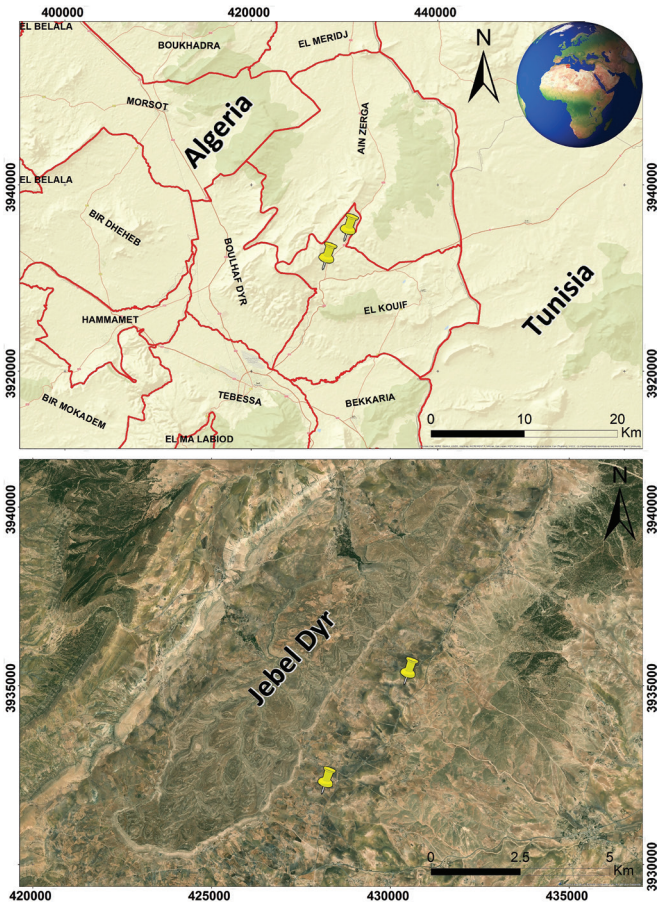

Figure 1. Geographic location of the study area.

2.2. Stratigraphy and the Phosphorites Occurrences

The lithostratigraphic facies range from Cretaceous to Neogene. Locally, the Paleocene-Eocene formations (Fig. 2) encountered in the Jebel Dhyr syncline (Bles, Fleury 1970) are:

a- Danian "e1": Made up of 75 to 100 m of gray clayey limestone, in small beds with wavy surfaces, alternating with gray marls rich in *Globigerina microfauna*.
b- Montian "e2-3": composed of more than 200 m of gray, homogeneous marl, at the top of which appear rare beds of gray clayey limestone rich in *lumachelle* with *oysters* and *Globorotalia*.
c- Thanetian "e4": Made up of 20 m of clayey limestone and phosphatic limestone. The exploitable layer of phosphates consists of two beds 1 to 2 m thick each, rich in numerous *Selachian* teeth.
d- Lower Lutetian - Ypresian "e5-6": composed of 150 m of massive limestone beds, with flint, *oysters* and *lumachelles* of Nummulites, alternating with softer limestone levels.
e- Continental Miocene "mc": made up of conglomerates with cemented calcareous elements, variegated clays and *Dinotherium* remains.

3. Materials and Methods

In order to examine the geological context and gather representative samples of phosphatic rocks in the study area, a fieldwork expedition was carried out. A total of 22 samples were carefully collected from Paleocene-Eocene phosphatic outcrops situated along the southern, eastern, and western escarpments of the Jebel Dhyr syncline. This sampling strategy aimed to ensure a diverse representation of phosphatic formations within the study area, enabling a thorough analysis of their petrographical, mineralogical, and geochemical properties. The collected samples serve as valuable specimens to advance our understanding of the phosphatic rocks in this region (Fig. 3).

Petrographic studies were performed using a polarizing optical microscope of the Leica DMLP type. Thin and polished sections were prepared to facilitate detailed petrographic analysis.

Geochemical analysis of the collected samples was conducted to determine the major elements using Perkin Elmer flame atomic absorption spectrometry. The samples were initially dissolved by melting with strontium metaborate and then further dissolved in 2% nitric acid. Fluorine content was measured using a potentiometer after mobilizing this element with concentrated hydrochloric acid. A Metrohm instrument equipped with a specific fluorine electrode was utilized for this purpose. Loss on ignition was determined through calcination at 1000°C.

The used protocol for XRD analysis for the mineralogical identification of phosphorites involves following

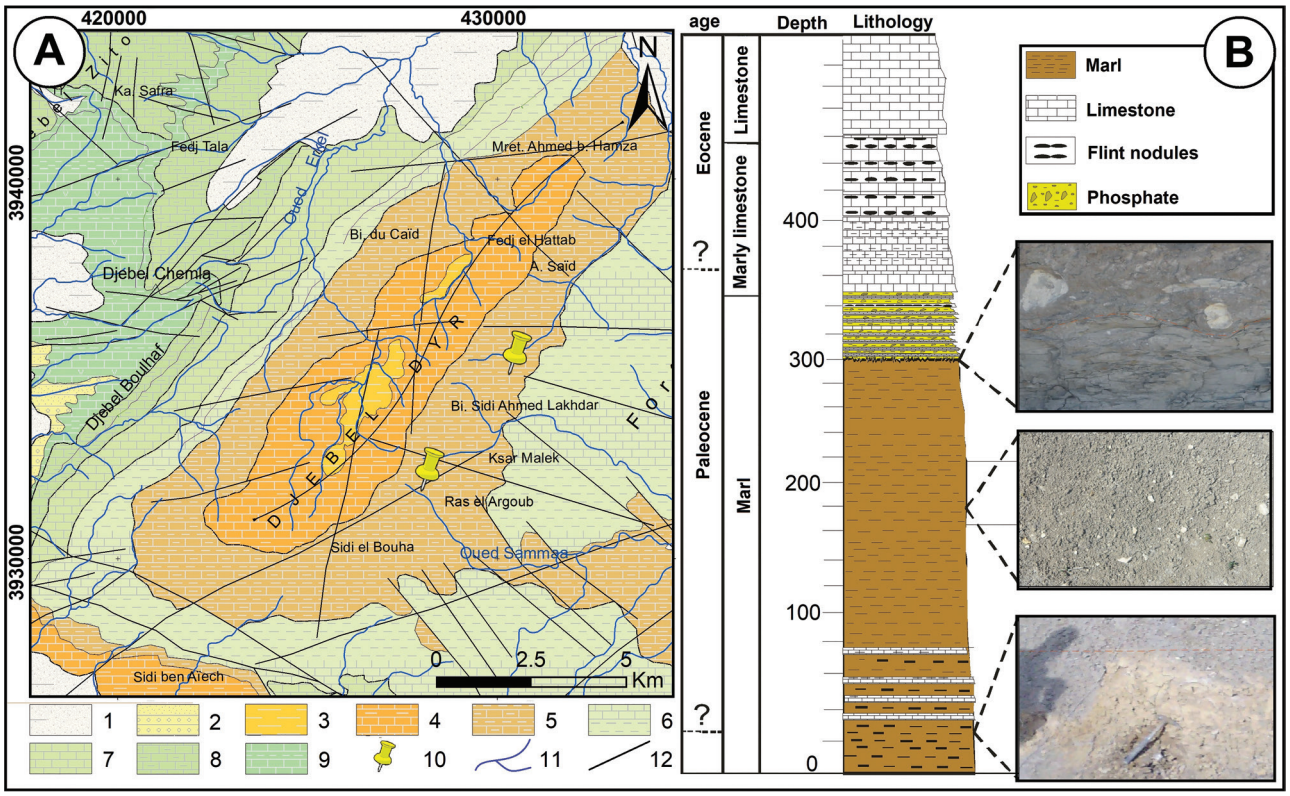

Figure 2. A: Simplified geological map of the Jebel Dhyr syncline; B: Lithostratigraphic log of Jebel Dhyr. [Legend of the geological map: 1= Holocene: Current and recent alluvium, scree slopes, piedmont accumulation, molasses. 2= Plio-Quaternary: Pebbles (sandstone and conglomerates) and marls. 3= Upper Lutetian: Marls, clays and conglomerates. 4= Ypresian, Lower Lutetian: Limestone with flint and marl-limestone, sometimes with gypsum. 5= Paleocene-Maastrichtian: Marl and marl-limestone. 6= Campanian, Maastrichtian: Marly at the base and varied limestone (oolitic, organogenic, flint) at the top. 7= Coniacian and Santonian: Limestones. 8= Turonian: Limestones and marls. 9= Cenomanian: Yellow limestone, marl and gypsum and dolomites. 10= Samples. 11= Streams. 12= Faults].

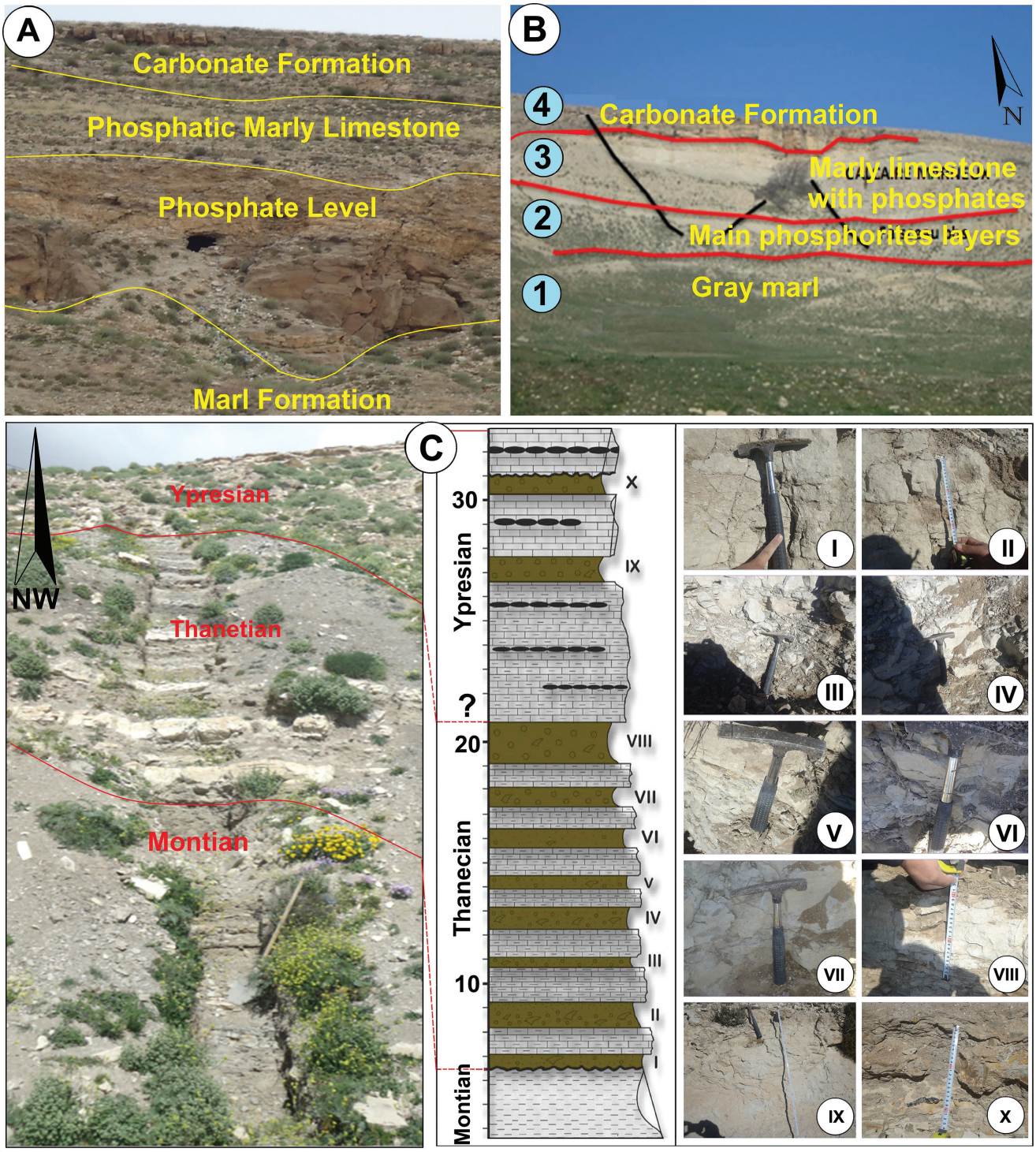

Figure 3. Panoramic view of the flanks of the Jebel Dhyr syncline; A: extreme southeast flank, B: southwest flank; C: The outcrops of the ten phosphate levels (Phosphorites and Marly limestone phosphates) sampled from Jebel Dhyr Syncline.

key steps. Initially, friable phosphatic sediments are processed to extract phosphatic allochem grains, including pellets, coprolites, intraclasts, and shark teeth, using an optimized screening method after simple disintegration. The disintegrated sediments are then subjected to sieve analysis using metallic sieves following the ASTM standard (ASTM D6913). After careful sorting under binoculars, the phosphatic grains, such as pellets, coprolites, granules, and fish teeth, are isolated and crushed to a particle size of 0.3 mm.

Next, X-ray diffraction measurements of the natural samples, in the form of multiphase powder, are recorded using an X'Pert Pro PANalytical diffractometer operating at 45 kV and 40 mA with Cu Kα radiation. The samples are scanned in the 2θ range from 5 to 75° (2θ) with a step size of 0.017°/s per step.

For the identification and quantification of different crystalline phases, a standard acquisition approach is employed, with parameters set at a step size of 0.02° and a time/number of scans of 20s. The resulting X-ray data are then interpreted using the "HighScore Plus" software. This conventional XRD protocol provides valuable information about the mineralogical composition of phosphorite samples, aiding in the accurate identification and characterization of the crystalline phases present.

4. Results and Discussion

The geological cross-sections conducted along the outcrops of Jebel Dhyr provide insightful information about the composition and structure of the phosphorite deposits in the region. These sections reveal the presence of sub-tabular phosphorite layers, which are relatively friable and have a thickness of several decimetres. These phosphorite layers alternate with layers of limestone, marl-limestone, and flint limestone located at the uppermost section. The observed alternation of different rock formations signifies the complex sedimentary history and depositional environment of the Paleocene-Eocene era in this area. These findings contribute to a better understanding of the geological context and distribution of phosphorites within the Jebel Dhyr region (Fig. 2).

The collected samples are mainly distributed over sandy phosphorite, calcareous phosphorite, and phosphatic mudstone rocks. On the other hand, the phosphatic allochems are represented by the following particles (Fig. 4): coprolites of various shapes, pellets of arenite sizes, fish teeth completely phosphate of varying shapes, and intraclasts (granules), which are hard to break.

The petrographic examination revealed that the texture of the phosphate samples predominantly represented the grainstone facies (Fig. 5). Within this facies, all samples exhibited a high percentage of allochems compared to the matrix.

The dominant phosphatic particles in this facies were pellets, which lacked concentric structures and were commonly referred to as pseudo-ooliths (Fig. 2). These pellets varied in colour from brownish white to brown and even almost black, depending on the organic matter content. They displayed a structure-less, sub- to well-rounded shape, often oval, and were relatively uniform in size, with diameters ranging from 200 to 250 µm. The particles exhibited polished and smooth surfaces due to remobilization from the original depositional environment (Chabou-Mostefaioui 1987; Ben Hassen et al. 2011). The phosphatic ooids within the pellets sometimes contained multiple cores, and these cores were also coated ooids. Some pellets showed a relict structure of organic material and consisted of apatite, commonly referred to as “collophane” (Boulemia et al. 2021). Apart from the presence of pellets, the samples also contained coprolites, which are fossilized excrement particles. These particles, originating from fecal matter, exhibited a diverse array of shapes and sizes, often surpassing 250 µm and occasionally even extending to a few millimetres. Their colours varied, spanning from a pale yellowish hue to a deep, darker shade (Boulemia et al. 2015).

The phosphorites also contained intraclasts, which were characterized by angular to irregular shapes and had internal microstructures (up to 1 cm in diameter). Skeletal fragments, including bones and teeth, were observed within the phosphorites. These biogenic phosphates consisted of well-preserved triangular teeth derived from sharks. Petrographically, the internal part of the phosphate particles consisted of microcrystalline translucent apatite or noncrystalline (amorphous) material (Fig. 5). Some skeletal fragments were replaced by microcrystalline quartz, indicating silicification. Silicification was also observed in certain phosphate particles within the cherty phosphate horizon. The cement within the phosphorites was calcareous (sparite) and occasionally siliceous, resulting from diagenetic calcitization and partial silicification (Abed, Al Agha 1989; Dar et al. 2015).

The major element compositions of 14 phosphorite samples are presented in Table 1. The phosphate beds at Jebel Dhyr are generally compared to the Kouif phosphorite horizons in the northern-eastern parts of the Tebessa region (Boulemia et al. 2015). The P_2O_5 content exhibited a narrow range, varying from 20.60 wt% to 25.80 wt%. This limited range of P_2O_5 content in the studied samples is primarily attributed to the dominance of the apatite group. On the other hand, the beds exhibited higher CaO content, ranging from 32.00 wt% to 35.10 wt%. Phosphorites are predominantly composed of apatite minerals, which consist of phosphorus (P) and calcium (Ca). Additionally, a significant amount of calcium is present in the form of carbonates such as calcite and dolomite (Boulemia et al. 2021). The CO_2 content ranged from 10.7 wt% to 12.60 wt%. McConnell (1973) suggested that the carbonate anionic group partly substitutes for the PO_4 group in apatite. In the studied samples, CO_2 is mainly found in the carbonate and phosphate (francolite) facies.

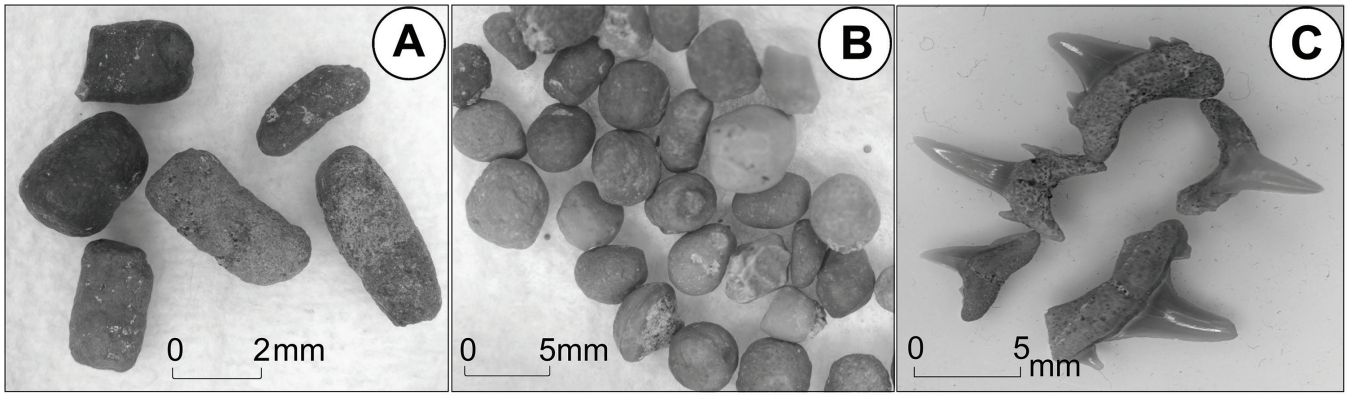

Figure 4. Photographs of the main allochems of Jebel Dhyr phosphorites illustrating A- Coprolith, B- Pellets, and C- Selachians Teeth.

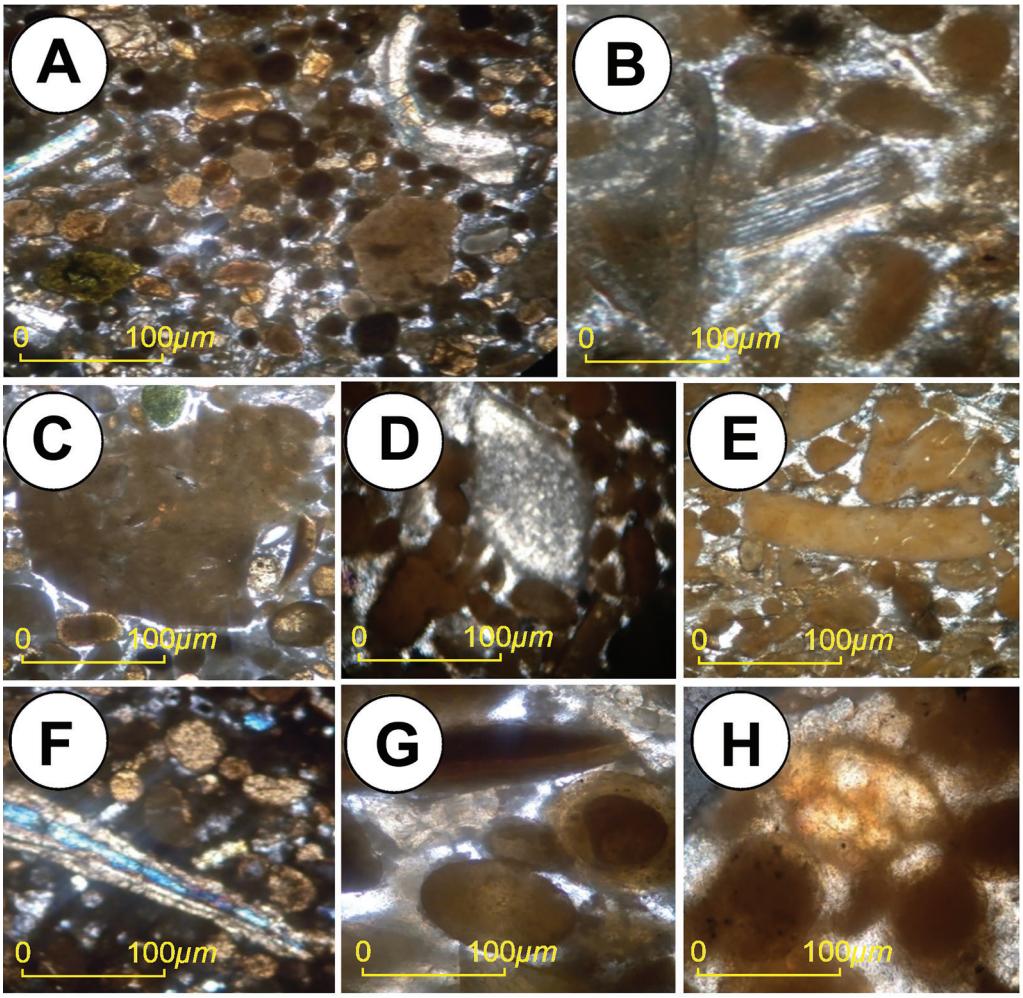

Figure 5. Texture of the phosphate samples: A- Bio-pellet phosphorite with a grainstone texture, featuring allochems represented by pellets, intraclasts, and bioclasts (bivalve arc and calcitic bone fragment), [200µm]. B- Bioclasts (vertebra and fish spine) within anisotropic granular phosphorite, [100µm]. C- Phosphatized blunt-edged intraclast (granule) surrounded by pellets and glauconite, [50µm]. D- Cryptocrystalline dolomite rhombohedron with an apatitic rim surrounded by grainstone pellets of various shapes, [50µm]. E- Cylindrical-shaped coprolite and brown-colored intraclast in grainstone textured phosphorite, [100µm]. F- Detrital quartz grains and quartz rim within the calcite-filled crack, [100µm]. G- Dispersed organic matter punctuates within pellets (concentric, non-nucleated, and oval) in a calcitic matrix, [50µm]. H- Globigerina acting as nuclei for a phosphatic ooid, surrounded by non-nucleated, organic-rich oval pellets, [50µm].

Table 1. The concentration of Geochemical elements (wt%) in phosphorites (bulk rock) samples from the Jebel Dhyr syncline, Eastern Algerian Atlas.

Sample ID	P_2O_5	CO_2	MgO	Na_2O	K_2O	CaO	SiO_2	Fe_2O_3	H_2O	Al_2O_3	SO_3	F	Tot. %
D1-I	23.17	10.7	1.84	0.71	0.13	35.1	9.7	0.66	1.62	0.77	11.85	2.6	98.85
D1-II	22.86	10.75	1.86	0.6	0.13	34.8	9.2	0.7	1.54	0.78	12.2	2.8	98.22
D1'-I	24.6	10.68	1.78	0.79	0.16	35.6	10.3	0.92	1.65	0.83	10.1	2.3	99.71
D2-II	23.4	10.65	1.8	0.7	0.15	35	9.5	0.91	1.62	0.81	11.1	3.7	99.34
D2-I	20.6	12.21	3	0.51	0.21	32	9.63	0.85	1.4	0.95	10.5	6.2	98.06
D3-II	20.2	11.8	2.7	0.55	0.21	34.2	9.05	0.82	1.5	0.93	10.6	5.9	98.46
D4-I	22.53	10.53	2.45	0.58	0.14	34.1	9.15	0.65	1.65	0.79	11.8	4.9	99.27
D4-II	20.8	11.6	2.5	0.59	0.12	33.9	9.1	0.6	1.7	0.74	11.9	4.6	98.15
D4'-I	21.9	11.7	2.9	0.6	0.11	34.1	9.1	0.55	1.75	0.72	11.95	3.2	98.58
D5-II	23.8	10.9	2.7	0.61	0.1	33.01	9.8	0.5	1.92	0.7	12.4	3.2	99.64
D6-I	24.6	12.6	2.35	0.52	0.12	32.2	9.1	0.85	1.58	0.74	10.8	3.2	98.66
D6-II	25.8	12.6	2.32	0.53	0.12	32.1	9.2	0.82	1.56	0.74	10.9	2.4	99.09
D8-I	21.8	11.33	2.69	0.6	0.17	32.7	10.6	1	1.63	0.86	12.1	4.4	99.88
D7-II	22.2	12.1	2.8	0.61	0.1	32.1	9.4	0.85	1.62	0.7	12.15	4.2	98.83

The MgO content in the samples varied from 1.80 wt% to 3.00 wt%. The lower MgO content suggests limited dolomitization and indicates the formation of phosphatic grains in low MgO seawater (Baioumy 2007). The silica phase (SiO_2) exhibited remarkable contents, ranging from 9.2 wt% to 10.3 wt%. The high

silica content in the chemical analysis is attributed to the presence of biogenic quartz and partial or complete silicification (chert) of certain layers (Boulemia et al. 2021). The concentrations of K_2O, Na_2O, Al_2O_3, and Fe_2O_3 were relatively low. This can be attributed to minor occurrences of clay minerals, which do not possess a phosphatic phase.

The SO_3 content was relatively high, ranging from 10.10 wt% to 12.40 wt%. Sulphur may occur in the apatite structure as a normal constituent of the phosphate lattice or in low amounts as gypsum, as detected by X-ray diffraction. The (PO_4) group in apatite can also be partially replaced by SO_4 (Stowasser 1975). The fluorine content ranged from 2.60 wt% to 6.20 wt%. Fluorine is present in the apatite lattice and can occur freely or in association with (OH) and O ions (McConnell 1973). Apparently, phosphorites of Jebel Dhyr syncline are more sulphurized and fluorinated than those of El Kouif locality (Boulemia et al. 2021).

The mineralogical analysis conducted reveals significant insights into the composition of the studied samples. The analysis indicates the presence of several mineral phases within the samples, shedding light on the diverse geological processes and environments that have influenced their formation. The identified minerals include prominent groups such as phosphates, sulphates, sulphides, tectosilicates, phyllosilicates, and native elements like graphite. These findings demonstrate the complex nature of the mineral assemblages found within the phosphorites of Jebel Dhyr. Furthermore, the results of the mineralogical analysis provide a foundation for further research into the origin, evolution, and potential applications of these mineral resources.

4.1. Bulk rock composition

The representative samples of phosphate from phosphatic layers were analysed using XRD. This showed that samples are mainly composed of apatite group (hydroxylapatite, francolite, fluorapatite, and dahllite), associated with carbonates (calcite, magnesium calcite, dolomite, and ankerite), silica (quartz and cristobalite - tridymite), sulphides (pyrite-cinnabar-covellite) and gypsum.

Hydroxylapatite $Ca_5(PO_4)_3(OH)$: The XRD of bulk rock phosphorite has shown the almost systematic presence of hydroxylapatite. The main lines of the mineral occurring in the studied diffractograms correspond to the lattice planes or most intense peaks as follows: (211), (300), (112), (202), (102), (210), (130), (222), (100), (312), (213), (200), (231), (140), (402), (004), (502) and (002). The predominant mineral occurs either single or associated with fluorapatite, francolite, and dahllite. Other non-phosphate minerals, gangue constituents' carbonates, silica, sulphates, and sulphides are coexisting.

Francolite $(Ca,Mg,Sr,Na)_{10}(PO_4,SO_4,CO_3)_6F_{2-3}$ is a carbonate-rich fluorapatite and has substitutions occurring in all sites (i.e., Ca, PO_4 and F sites; Jarvis et al. 1994). It appears at the phosphorite layers and is associated mainly with hydroxylapatite. Apparently, it features less quantitative dominance in our field compared to those of North Africa.

Fluorapatite $Ca_5(PO_4)_3F$: This mineral, associated with hydroxylapatite, is apparently mainly characterized by the wealthy bioclasts levels (tooth and bone fragments).

Dahllite $Ca_5(PO_4,CO_3)_3(OH,O)$: This mineral of calcium-phosphate presents sodium carbonate crystallographic parameters (a and c) relatively higher than those of other apatites (Table 2). The dahllite is rarely found in the XRD records associated with hydroxylapatite and quartz. Substitutions that affect the sedimentary apatite are frequent and directly influence the symmetry of the crystal lattice which result in changes to the parameters a and c. The decrease in the crystallographic parameter of the apatite may be due to the substitutions F-OH, O-2OH, Ca-Na, and PO_4-CO_3.

Carbonate sediments are composed mainly of calcite, ankerite, dolomite, and magnesium calcite. The calcite is characterized by its main line (104) at a distance of 3.036 Å. Sometimes the main peak (2Θ 29.395°) shows a slight shift towards higher angles (Fig. 6, Table 3). This displacement results from the incorporation of magnesium and/or iron in the calcite structure. Indeed, the magnesium calcite is marked to 2Θ 29.500°, dolomite to 30.815°, and ankerite to 30.918° (Table 3). Associations calcite-ankerite, calcite-dolomite, and magnesium calcite are recorded in the same samples that provide information on metasomatic phenomena — dolomitization. It is important to highlight that cherty layers are characterized by the presence of dolomite and magnesium calcite, which are often associated with tridymite. Furthermore, as was encountered rarely, a sodium aluminium carbonate hydroxide "dawsonite" $NaAl(CO_3)(OH)_2$, is associated with the zeolite and albite.

Quartz α is identified by its main line 3.33 Å at 2Θ 26.73°. It is often associated only with apatite (hydroxylapatite, francolite, fluorapatite, and dahllite) and sometimes

Table 2. Crystallographic parameters of the crystalline unit cell of apatite group in phosphorites from the Jebel Dhyr syncline, Eastern Algerian Atlas.

Mineral	a or b (Å)	C (Å)	c/a	Vol. of unit cell	Chemical formula
fluorapatite	9.371	6.885	0.734	523.12	$Ca_5(PO_4)_3F$
hydroxylapatite	9.352	6.882	0.735	521.26	$Ca_5(PO_4)_3(OH)$
francolite	9.340	6.880	0.736	519.77	$(Ca,Mg,Sr,Na)_{10}(PO_4,SO_4,CO_3)_6F_{2-3}$
dahllite	9.450	6.885	0.725	532.09	$Ca_5(PO_4,CO_3)_3(OH,O)$

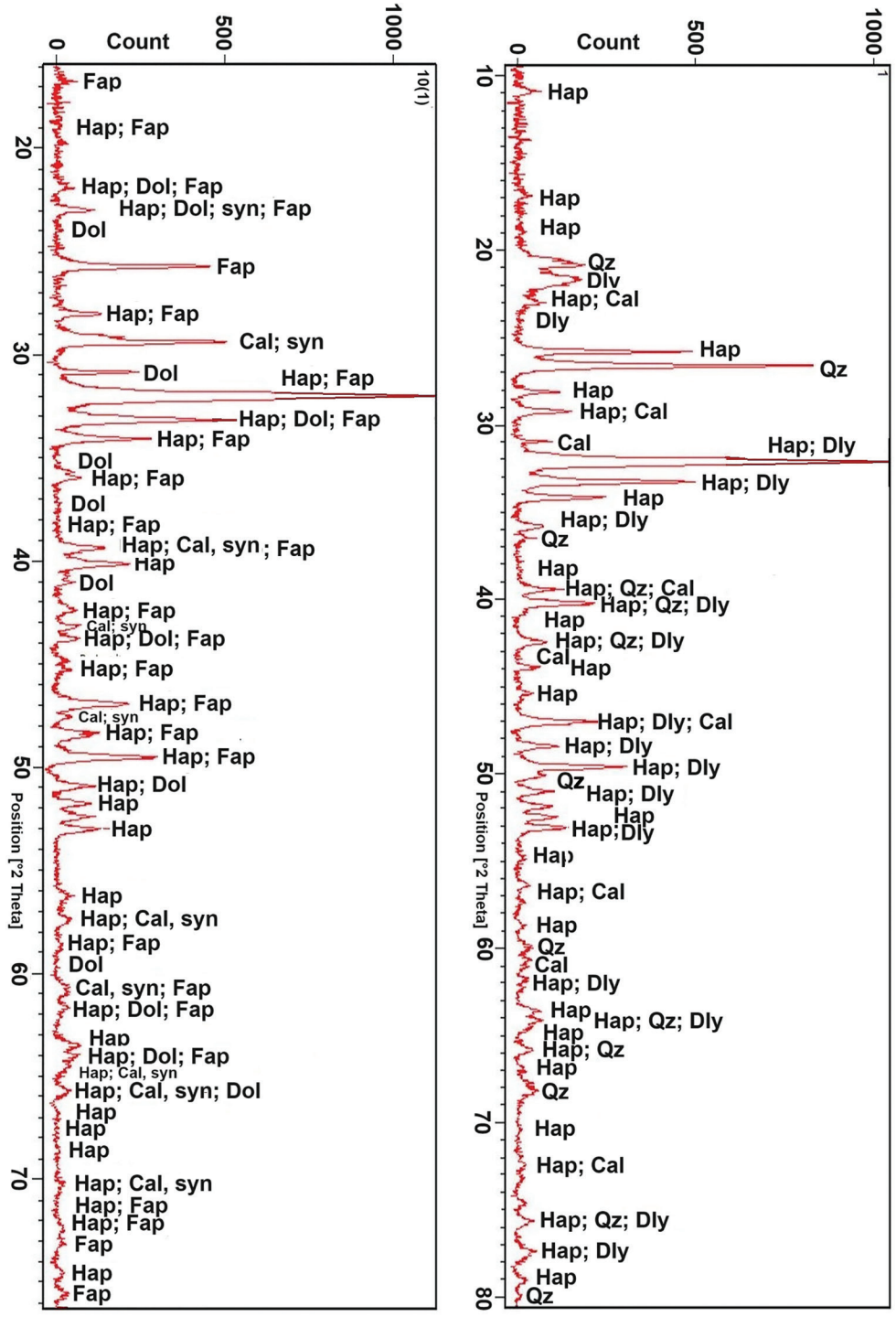

Figure 6. Examples of X-ray diagram for phosphorite sample show the apatitic different component with carbonates and siliceous gangue of Jebel Dhyr syncline. Abbreviations after Warr (2021; IMA–CNMNC).

Table 3. X-ray diffraction parameters of carbonate group in phosphorites from Djebel Dhyr syncline, Eastern Algerian Atlas.

Mineral	hkl	d (Å)	2Θ [deg]	Geochemical formula
calcite	104	3.0360	29.395	$CaCO_3$
magnesian calcite	104	3.0254	29.500	$(CaMg)CO_3$
dolomite	104	2.8893	30.815	$CaMg(CO_3)_2$
ankerite	104	2.8890	30.918	$Ca(Fe,Mg)(CO_3)_2$

in the presence of ankerite. It is probably of a detrital origin. However other varieties of silice (cristobalite-tridymite) met in high levels in cherty levels (interbed the dolomitic phosphates layers) accompanied dolomite and magnesium calcite. It is probably of a biochemical origin (Fig. 6).

Gypsum is recognized by its main diffraction peaks at 2Θ values of 11.59°, 20.74° and 29.16°. It is encountered in diffractograms, and observed at a single phosphatized sample, fluorine-sodium sulphate $Na_3Ca_2(SO_4)_3F$ associated with graphite (Fig. 7, right). Presumably, the gypsum is of secondary type. This can result, in an arid climate, precipitation of rain water enriched with sulphates when runoff from overlying formations. Especially, the evaporite formations, which are one of the traits that characterize this region of diapirs of Algerian-Tunisian border.

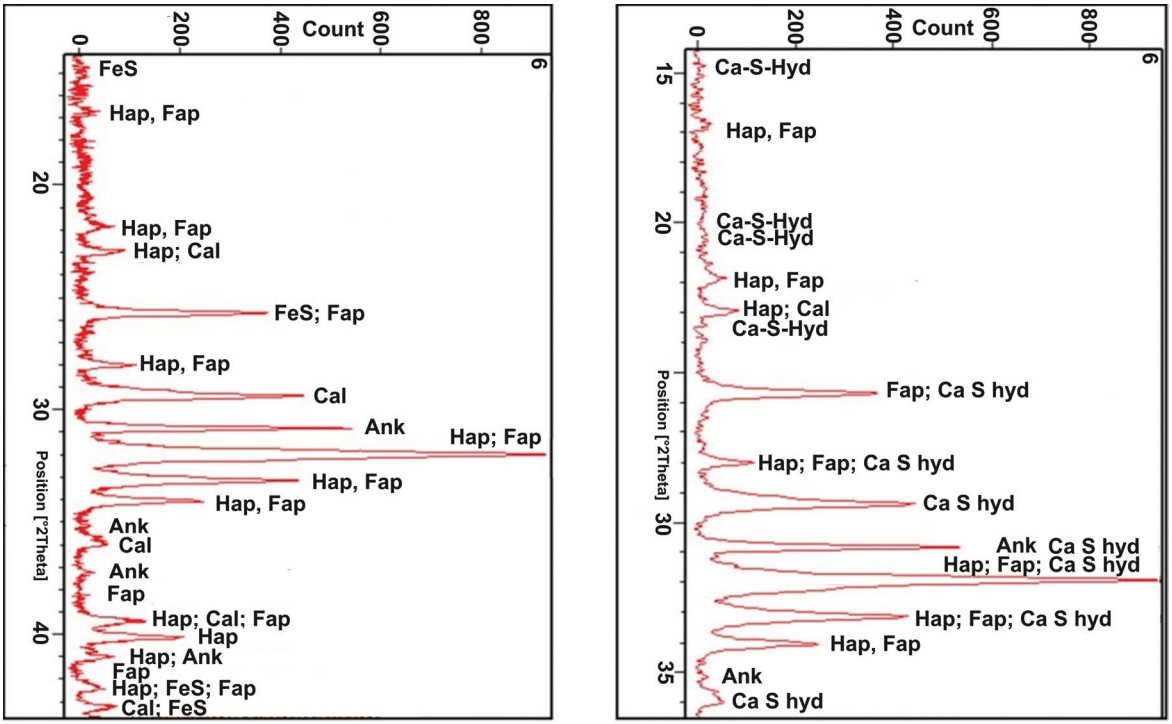

Figure 7. Examples of X-ray patterns showing the presence of sulphides and sulphates in phosphorites samples from Jebel Dhyr syncline.

Sulphides: pyrite-cinnabar-covellite apparently, with low amounts (in traces) are detected on the X-ray records of different samples of the same vertical profile by well individualized peaks (Fig. 7, left). In fact, due to the presence of sulphate (SO_3) ions in the water, the pyrite could be precipitated at the time of phosphatization.

Zeolites (alumina silicates hydrated minerals): occasionally observed on the diffractograms are: cowlesite ($CaAl_2Si_3O_{10}{\cdot}6H_2O$), yugawaralite ($CaAl_2Si_6O_{16}{\cdot}4H_2O$), and offretite ($KCaMg(Si_{13}Al_5)O_{36}{\cdot}15H_2O$). Indeed, these zeolites have seen associated with palygorskite and albite in the presence of apatite, (Fig. 8).

Clays; palygorskite $(Mg,Al)_2Si_4O_{10}(OH){\cdot}4(H_2O)$ was the sole encountered phyllo-silicates. It was recognized by its main line position (peak) with d (10.12 Å) at 2Θ 8.73° on diffractograms. The other clay types are absent which requires a priori oriented thin section, heated and glycolic, (Fig. 8, left).

Feldspar: albite $(Na,Ca)(Si,Al)_4O_8$, is detected and occasionally associated with yugawaralite and dawsonite. This alumino-sodic mineral shows its maximum intensity at 2Θ 29.7°. Its magmatic origin seems more logical, especially in the presence of zeolites (Fig. 8, right).

Graphite: This carbon hexagonal system is recognized by its main peak (002) at 2Θ 26.6°. Its presence is rarely associated with apatite fluoride and hydroxylapatite. Its existence indicates a confined environment rich in organic matter.

The existence of minerals such as zeolites, palygorskite, dawsonite and sodium-fluorinated sulphate in the study area is due to the enrichment of the depositional environment in sodium, aluminum, magnesium, potassium and silica. The origin of this type of minerals in the Tebessa-El Kasserine collapsed basin is very controversial, but the most likely is the volcanic origin as interpreted by Sassi (1974) in the Gafsa mining basin.

Table 4 provides a summary of mineral phases identified by light microscopy, X-ray diffraction studies and macroscopics observations, in phosphorites from Jebel Dhyr syncline.

4.2. Phosphatic allochem grains

The analyzed samples from the phosphorite layer consisted of representative allochems, including teeth, coproliths, granules, and pellets. XRD analysis revealed that these specimens were predominantly composed of apatites, with the exception of a few phosphatic pellets. The following are the obtained results:

Bioclasts are represented by fossil fish teeth (Salesians) of variable sizes and shapes and which are in the majority completely phosphated. XRD performed on samples of teeth from phosphates layers of Jebel Dhyr has overwhelmingly demonstrated the systematic presence of fluorapatite, $Ca_5(PO_4)_3F$.

Intraclasts and granules: They are hard to crack, beige or gray with a black patina and similar to large gravels and are not characterized by any typical shape. Diffractometry on granules (greater than 10 mm) of different shapes and sizes indicated that the latter are represented by the hydroxylapatite associated with fluorapatite or francolite (Fig. 9).

Coprolits: particles greater than 2 mm, fossil's of fecal origin, recognized widely of various shapes (Fig. 10, right). Coprolites are found in the state of fragments,

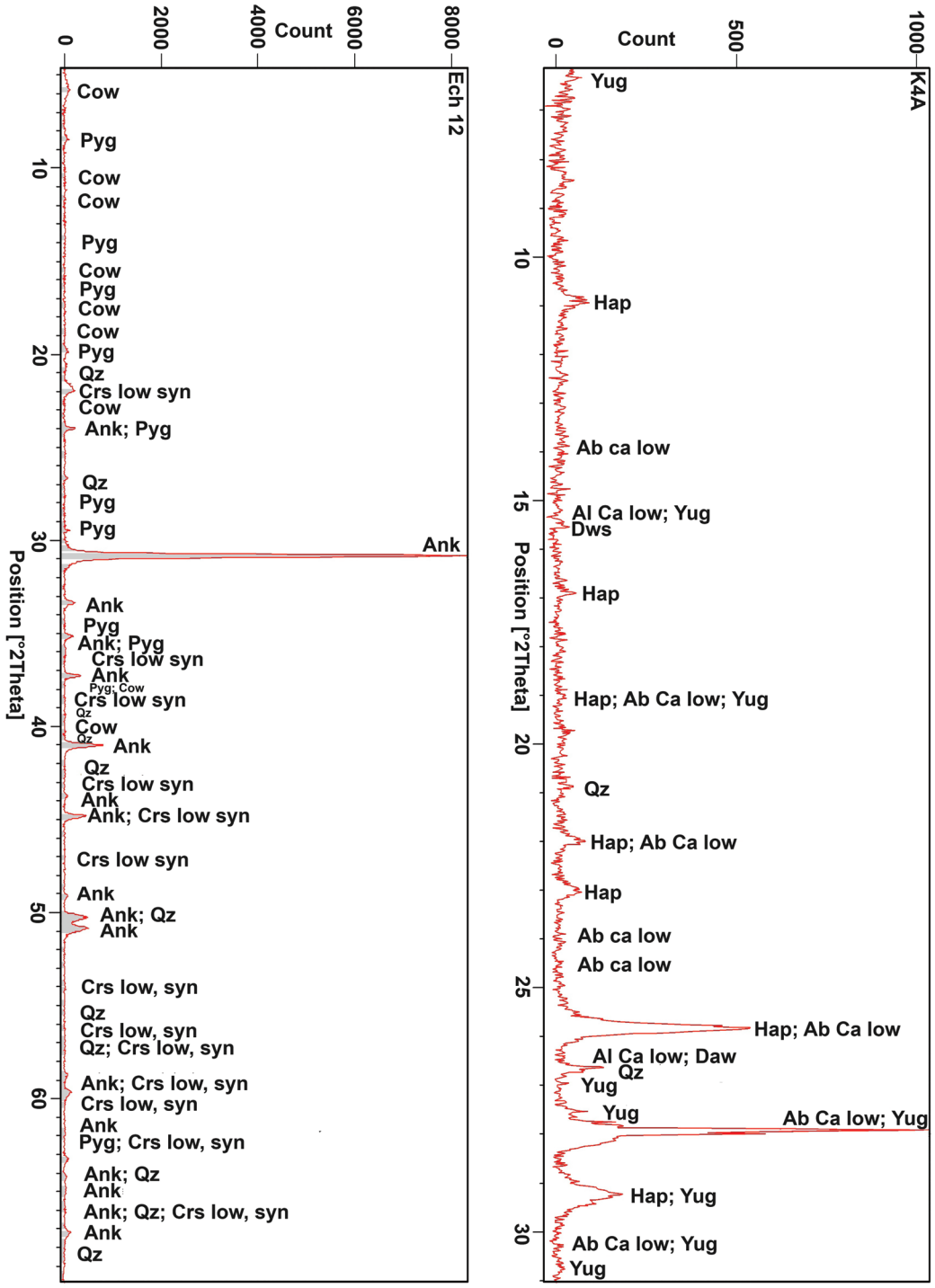

Figure 8. XRD diffractograms of fine fraction phosphorite samples from Jebel Dhyr syncline showing zeolites, feldspars and clays.

Table 4. Recapitulation of mineral phases identified by light microscopy, X-ray diffraction and macroscopics observations, in phosphorites from the Jebel Dhyr syncline, Eastern Algerian Atlas.

Mineral groups encountered	Sampling type	
	Bulk rock	Phosphatic allochems grains
apatite (hydroxylapatite, fluorapatite, francolite, dahllite*)	++	++
Carbonates (calcite, dolomite, magnesian calcite*, ankerite*, dawsonite*)	++	--
Sulfates (gypsum)	+	--
Sulfides (pyrite*-cinnabar*-covellite*)	+	--
Tectosilicates (quartz)	++	+
Tectosilicates (feldspar, zeolite*)	+	--
Clays (palygorskite*)	++	--
Native element (graphite)	+	--

AAAA* : Mineral detected only by XRD

++: abundant +: present --: absent

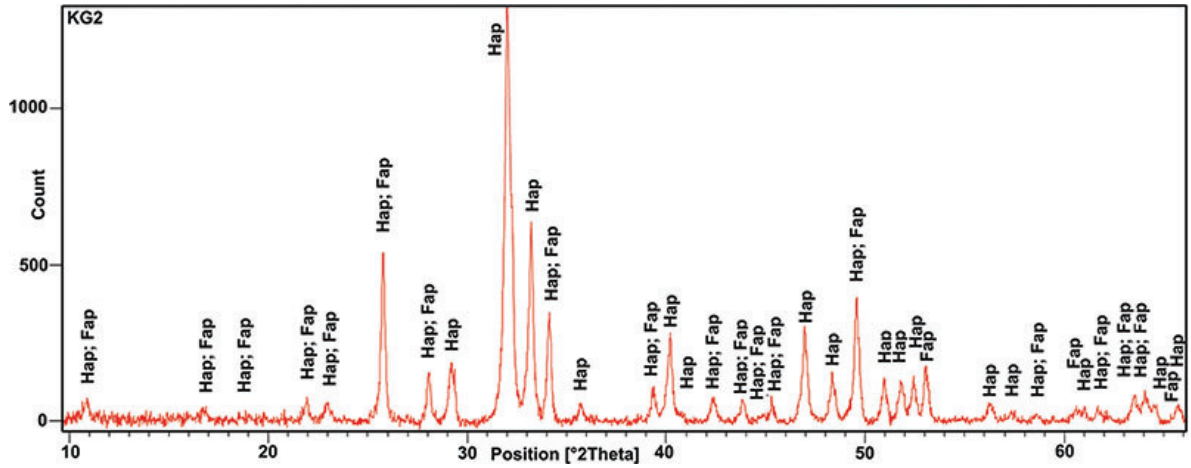

Figure 9. Diffractogram of a phosphate granule sample from the Jebel Dhyr syncline.

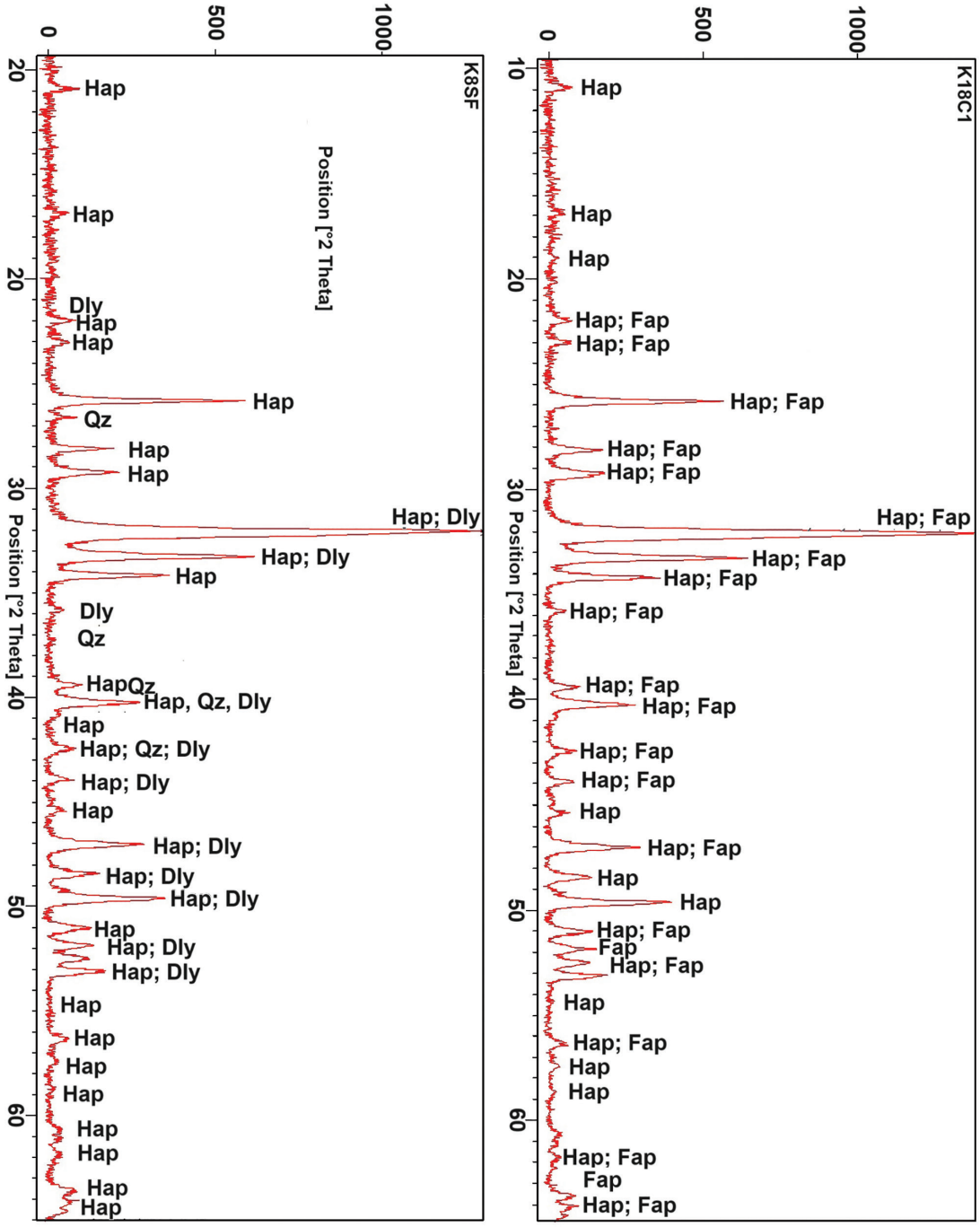

Figure 10. Left: Diffractogram of isolated pellets, Right: Diffractogram of isolated coprolites from the Jebel Dhyr syncline.

Table 5. Comparative X-ray diffraction parameters (d_{hkl}) of apatite group from phosphorites deposits in North Africa.

(hkl) (Miller index)	d_{hkl} of peaks (Å)			
	J. Jebs, Tunisia (Beji-Sassi 1984)	Foum Selja,Tunisia (Chaabani 1978)	Morocco (El Haddi 2014)	Dhyr, Algeria (this study)
100	8.164	8.15	8.074	8.099
101	5.281	5.29	5.250	5.244
200	4.052	4.04	4.041	4.049
111	3.873	3.87	3.862	3.867
002	3.456	3.45	3.444	3.441
102	3.183	3.17	3.170	3.167
120	3.062	3.05	3.051	3.061
211	2.792	2.79	2.792	2.796
112	---	2.78	2.771	2.771
300	2.695	2.69	2.693	2.699
202	2.627	2.62	2.622	2.622
301	2.507	2.51	2.510	2.513
122	2.284	2.28	2.282’	2.287
310	2.240	2.24	2.240	2.240
131	2.130	2.13	2.131	2.135
113	2.062	2.07	2.061	2.059
203	1.997	----	1.996	1.995
222	1.931	1.93	1.930	1.933
132	1.879	1.87	1.880	1.880
123	1.836	1.84	1.836	---
231	1.788	1.77	1.790	1.790
410	1.762	1.76	1.765	1.766
303	1.741	1.73	1.743	---
004	1.722	1.71	1.723	1.720
322	---	---	1.632	1.634

thus supporting the hypothesis of the reworking at the origin of the accumulations of phosphorites. XRD analysis performed on isolated forms showed that coprolits consist of hydroxylapatite and fluorapatite, sometimes associated with dahllite.

Phosphatic pellets: These arenite-and lutite-sized particles are spheric and/or ovoid in shape. These pellets carry organic matter at various rates, which is evident in their color ranging from light yellow to very dark or even opaque brown. The XRD analysis carried out on the powder of the (0.1-0.125 mm) sand fraction separated from the friable phosphorites revealed a mineralogical composition of hydroxylapatite and fluorapatite, sometimes associated with dahllite, in the presence of quartz (Fig. 10, left). Indeed, the presence of other non-phosphated mineral phases such as quartz was observed. This could be explained by the existence of non-apatitic minerals serving as nuclei for these ooids (type of pellets) with apatitic cortex.

The phosphorites investigated in the Jebel Dhyr syncline exhibit a homogeneous mineral composition, primarily comprising hydroxylapatite, fluorapatite, francolite, and dahllite. These apatite minerals display similar diffractometric characteristics, as shown by the hkl and d values in Table 5, with minor variations. The results suggest that the spatiotemporal distribution has minimal influence on the diffractometric properties. Regardless of sample location, X-ray analysis consistently reveals a remarkable consistency in the positions of the primary apatite diffraction lines, with only slight deviations within a few tenths of a degree.

5. Conclusions

The phosphorites of the Jebel Dhyr syncline are commonly interbedded with limestones, shales, and occasionally cherts. Petrographic examination of the phosphorites reveals similarities with the phosphates of the El Kouif locality, albeit with minor differences in the abundance of phosphatic particles and the nature of the orthochems. In fact, pellets, coprolites, bioclasts (including bone and teeth) and phosphatized intraclasts are relatively more present in Dhyr phosphorites than those of El Kouif locality. Moreover, the clayey and siliceous matrix is more predominant than calcareous (calcitic and dolomitic) cement in Dhyr phosphorites. Furthermore, the content of organic matter is with the same distribution within the various phosphate beds.

The high concentrations of P_2O_5 and CaO in the phosphorites indicate a greater abundance of apatite constituents. The sulphur content is associated with francolite and secondary gypsum formation. Additionally, significant amounts of calcium are present in carbonates such as calcite and dolomite. The low concentrations of K_2O, Na_2O, Al_2O_3, and Fe_2O_3 oxides may be attributed to minor occurrences of clay minerals.

The Paleocene-Eocene phosphorites samples of the Jebel Dhyr syncline were analyzed using the XRD technique to identify the multiphase structure and crystallographic parameters. The analysis of the bulk rock pattern, enriched in phosphate grains, enabled the identification of the phosphatic phase represented by the apatite group, which includes hydroxylapatite ($Ca_5(PO_4)_3OH$) as the most widespread species, as well as dominant francolite. The presence of francolite indicates the significant presence of carbonates in the phosphatic rocks. Other phosphatic components, such as fluorapatite, $Ca_5(PO_4)_3F$ and dahllite, are mainly found in levels rich in bioclasts. Substitutions affecting sedimentary apatite are common and directly impact the crystal lattice symmetry. These apatitic components are primarily associated with carbonates (calcite-dolomite-ankerite) and/or silica, which form variable exogenous gangue. Associations such as calcite-ankerite, calcite-dolomite-calcite, and magnesium calcite were observed in the same samples, providing information on metasomatic phenomena such as dolomitization and dedolomitization.

At the cherty passages, opal-CT associated with dolomite is the main mineral. The enrichment in opal suggests high silica content in the depositional environment during the formation of these layers, possibly due to contributions from organisms with siliceous tests (radiolarians, diatoms, etc.).

Additionally, non-phosphate phases, including evaporated minerals (gypsum) and sulphide minerals (pyrite, cinnabar, and covellite), are observed in low representation in some samples. The presence of iron-sulphur and copper-sulphur minerals in the phosphatic rocks indicates highly reducing conditions during their formation. The presence of graphite (carbon) indicates anoxic conditions associated with phosphorite genesis.

The existence of minerals such as zeolites, palygorskite, dawsonite, and sod-fluorinated sulphate in the Tebessa-El Kasserine collapsed basin suggests environmental enrichment of sodium, aluminum, magnesium, potassium, and silica. Under favourable physicochemical conditions, these elements can combine to form these types of minerals. The origin of these chemical elements is likely associated with the alteration of igneous rocks, specifically ophites, found in the Tebessa region.

Allochems, which are various phosphatic components or grains separated from the phosphorites of the Jebel Dhyr syncline, include phosphorite pellets, phosphatized fossil teeth, coproliths, and granules. These constituents are dispersed within the clay matrix of these deposits. XRD analysis conducted on phosphatic allochems powder revealed a mineralogical composition consisting of hydroxylapatite with francolite or fluorapatite, sometimes associated with dahllite. Pelletal phosphorites are particularly common, and some are occasionally associated with quartz, suggesting the existence of non-apatitic cores serving as nuclei for these pellets with an apatitic cortex. This mineralogical composition, as highlighted by XRD analysis, is recorded for the first time in the phosphorites of the Jebel Dhyr syncline. These results demonstrate certain consistency regardless of the spatiotemporal distribution of the samples. In sum, with great mineralogical similarities, the phosphorites on Jebel Dhyr syncline belong to the same family as one of the Algerian deposits

Acknowledgements

This work was overseen by the IAWRSMB - Tunisia and the Laboratory of Applied Research in Engineering Geology, Geotechnics, Water Sciences, and Environment, Setif 1 University, Algeria. Acknowledgments to the Research Unit of the Faculty of Sciences of Tunis for the technical support. Tribute to the editor and reviewers for their valuable improvement on the manuscript.

Conflict of interest statement

On behalf of all authors, the corresponding author states that there is no conflict of interest. No participating authors have a financial or personal relationship with a third party whose interests could be influenced by the article's content. The corresponding author ensures that the descriptions are accurate and agreed upon by all authors.

References

Abed, A. M., & Al-Agha, M. R. (1989). Petrography, geochemistry and origin of the NW Jordan phosphorites. *Journal of the Geological Society*, *146*(3), 499-506. https://doi.org/10.1144/gsjgs.146.3.0499

Abed, A. M., Arouri, K. R., & Boreham, C. J. (2005). Source rock potential of the phosphorite–bituminous chalk–marl sequence in Jordan. *Marine and Petroleum Geology*, *22*(3), 413-425. https://doi.org/10.1016/j.marpetgeo.2005.01.004

Abou El-Anwar, E., & Abd El Rahim, S. (2022). Mineralogy, geochemistry and origin of the phosphorites at Um El-Huwtat mine, Quseir, Central Eastern Desert. *Egypt Carbonates and Evaporites 37*:16. https://doi.org/10.1007/s13146-022-00759-4

Anis, Z., Wissem, G., Riheb, H., Biswajeet, P., & Essghaier, G. M. (2019). Effects of clay properties in the landslides genesis in flysch massif: Case study of Aïn Draham, North Western Tunisia. *Journal of African Earth Sciences*, *151*, 146-152. https://doi.org/10.1016/j.jafrearsci.2018.12.005

ASTM International. (2017). Standard Test Methods for Particle-Size Distribution (Gradation) of Soils Using Sieve Analysis (ASTM D6913-17). ASTM International.

Bagwan, W. A., Gavali, R. S., & Maity, A. (2023). Quantifying soil organic carbon (SOC) density and stock in the Urmodi River watershed of Maharashtra, India: implications for sustainable land management. *Journal of Umm Al-Qura University for Applied Sciences*, *9*, 548-564. https://doi.org/10.1007/s43994-023-00064-3

Baioumy, H. M. (2007). Iron–phosphorus relationship in the iron and phosphorite ores of Egypt. *Geochemistry*, *67*(3), 229-239. https://doi.org/10.1016/j.chemer.2004.10.002

Barra, P. J., Pontigo, S., Delgado, M., Parra–Almuna, L., Duran, P., Valentine, A. J., Jorquera, M. A., & Mora, M. de la L. (2019). Phosphobacteria inoculation enhances the benefit of P–fertilization on *Lolium perenne* in soils contrasting in P–availability. *Soil Biology and Biochemistry*, *136*, 107516. https://doi.org/10.1016/j.soilbio.2019.06.012

Béji Sassi, A. (1984). Petrology, Mineralogy, and Geochemistry of Phosphatic Sediments from the Eastern Edge of Kasserine Island (Tunisia). Doctoral Thesis, 3rd Cycle, University of El Manar.

Ben Hassen, A., Trichet, J., Disnar, J. R., & Belayouni, Y. (2011). Pétrographie et géochimie comparées des pellets phosphatés et de leur gangue dans le gisement phosphaté de Ras-Draa (Tunisie). Implications sur la genèse des pellets phosphatés. *Swiss Journal of Geosciences*, *103*, 457-473. doi: 10.1007/s00015-010-0029-x

Benmarce, K., Hadji, R., Zahri, F., Khanchoul, K., Chouabi, A., Zighmi, K., & Hamed, Y. (2021). Hydrochemical and geothermometry characterization for a geothermal system in semiarid dry climate: The case study of Hamma spring (Northeast Algeria). *Journal of African Earth Sciences*, *182*, 104-285. https://doi.org/10.1016/j.jafrearsci.2021.104285

Besser, H., Dhaouadi, L., Hadji, R., Hamed, Y., & Jemmali, H. (2021). Ecologic and economic perspectives for sustainable irrigated agriculture under arid climate conditions: An analysis based on environmental indicators for southern Tunisia. *Journal of African Earth Sciences*, *177*, 104-134. https://doi.org/10.1016/j.jafrearsci.2021.104134

Bles, JL. & Fleury, J. (1970). Notice explicative de la carte géologique du Morsot (178). Service géologique de l'Algérie Alger, 1-36.

Boubazine, L., Boumazbeur, A., Hadji, R., & Fares, K. (2022). Slope failure characterization: A joint multi-geophysical and geotechnical analysis, case study of Babor Mountains range, NE Algeria. *Mining of Mineral Deposits*, *16*(4), 65-70. https://doi.org/10.33271/mining16.04.065

Boulemia, S., Hadji, R., & Hamimed, M. (2021). Depositional environment of phosphorites in a semiarid climate region, case of El Kouif area (Algerian–Tunisian border). *Carbonates and Evaporites*, *36*(3), 1-15. https://doi.org/10.1007/s13146-021-00719-4

Boulemia, S., Hamimed, M., Bouhlel, S., & Bejaoui, J. (2015). Petro-Mineralogical Analysis of Sedimentary Phosphate of Marine Origin, Case of the Locality of El Kouif (Algerian-Tunisian Confines). *Open Journal of Geology*, *5*, 156-173. http://dx.doi.org/10.4236/ojg.2015.53015

Brahmi, S., Baali, F., Hadji, R., Brahmi, S., Hamad, A., Rahal, O., ... & Hamed, Y. (2021). Assessment of groundwater and soil pollution by leachate using electrical resistivity and induced polarization imaging survey, case of Tebessa municipal landfill, NE Algeria. *Arabian Journal of Geosciences*, *14*(4), 1-13. https://doi.org/10.1007/s12517-021-06571-z

Buccione, R., Kechiched, R., Mongelli, G., & Sinisi, R. (2021). REEs in the North Africa P-Bearing Deposits, Paleoenvironments, and Economic Perspectives: A Review. *Minerals*, *11*(214), 1-27. https://doi.org/10.3390/min11020214

Chaabani, F. (1978). Phosphates of the Type Section of Foum Selja (Métlaoui, Tunisia): A Sequential Sedimentary Series with Paleogene Evaporites. Doctoral dissertation, University of Louis Pasteur, Strasbourg.

Chabou-Mostefaoui, S. (1987). Étude de la série phosphatée tertiaire du Jebel Onk, Algérie, Stratigraphie, Pétrographie, Minéralogie et Analyse Statistique [Unpublished doctoral dissertation, University of Aix-Marseille III, France].

Crosby, C. H., & Bailey, J. V. (2012). The role of microbes in the formation of modern and ancient phosphate mineral deposits. *Frontiers in Microbiology*, *3*:241. doi: 10.3389/fmicb.2012.00241

Dahoua, L., Usychenko, O., Savenko, V. Y., & Hadji, R. (2018). Mathematical approach for estimating the stability of geotextile-reinforced embankments during an earthquake. *Mining Science*, *25*, 207-217. doi: 10.5277/msc182501

Dar Shamim A., Khan K. F, & Birch W. D. (2017). Sedimentary: Phosphates, Reference Module in Earth Systems and Environmental Sciences, *Elsevier*, *24*, 1-17 doi: 10.1016/B978-0-12-409548-9.10509-3

Dar, S. A., Khan, K. F., Khan, S. A., Khan, S., & Alam, M. M. (2015). Petro-mineralogical studies of the Paleoproterozoic phosphorites in the Sonrai basin, Lalitpur District, Uttar Pradesh, India. *Natural Resources Research*, *24*(3), 339-348. doi: 10.1007/s11053-014-9260-x

El Bamiki, R., Raji, O., Ouabid, M., Elghali, A., Khadiri Yazami, O., & Bodinier, J.-L. (2021). Phosphate Rocks: A Review of Sedimentary and Igneous Occurrences in Morocco. *Minerals*, *11*, 1-23. https://doi.org/10.3390/min11101137

El Haddi, H. (2014). Silicifications of the Phosphate Series of Ouled Abdoun (Maastrichtian-Lutetian, Morocco): Sedimentology, Mineralogy, Geochemistry, and Genetic Context. Doctoral Thesis, Hassan II University of Casablanca, 135p.

Ferhaoui, S., Kechiched, R., Bruguier, O., Sinisi, R., Kocsis, L., Mongelli, G., Bosch, D., Ameur-Zaimeche, O., & Laouar, R. (2022). Rare earth elements plus yttrium (REY) in phosphorites from the Tébessa region (Eastern Algeria): Abundance, geochemical distribution through grain size fractions, and economic significance. *Journal of Geochemical Exploration*, *241*, 107058.

Flandrin, J. (1948). Contribution à l'étude stratigraphique du Nummulitique algérien. *Bulletin du Service de la Carte géologique de l'Algérie*, 19, 1-340.

Fleet, M.E. & Liu, X. (2005) Local structure of channel ions in carbonate apatite. *Biomaterials*, *26*, 7548–7554. https://doi.org/10.1016/j.biomaterials.2005.05.025

Fleury, J. (1969). Stratigraphie du Crétacé et de l'Eocène (Aptien à Lutétien) de la feuille 1:50000 morsot, no 178. *Publications du Service de la Carte géologique de l'Algérie, Nouvelle série Bulletin*, *39*, 145-157.

Fredj, M., Hafsaoui, A., Riheb, H., Boukarm, R., & Saadoun, A. (2020). Back-analysis study on slope instability in an open pit mine (Algeria). *Naukovyi Visnyk Natsionalnoho Hirnychoho Universytetu*, *2*, 24-29.

Gadri, L., Hadji, R., Zahri, F., Benghazi, Z., Boumezbeur, A., Laid, B. M., & Raïs, K. (2015). The quarries edges

stability in opencast mines: a case study of the Jebel Onk phosphate mine, NE Algeria. *Arabian Journal of Geosciences*, *8*(11), 8987-8997.

Gál, P., Polgári, M., Józsa, S., Gyollai, I., Kovács, I., Szabó, M., & Fintor, K. (2020). Contribution to the origin of Mn-U-Be-REE-enrichment in phosphorite, near Bükkszentkereszt, NE Hungary. *Ore Geology Reviews*, *125*, 103665. https://doi.org/10.1016/j.oregeorev.2020.103665

Garnit, H., Bouhlel, S., & Jarvis, I. (2017). Geochemistry and depositional environments of Paleocene-Eocene phosphorites: Metlaoui Group, Tunisia. *Journal of African Earth Sciences*, *134*, 704-736. https://doi.org/10.1016/j.jafrearsci.2017.07.021

Hamad, A., Abdeslam, I., Fehdi, C., Badreddine, S., Mokadem, N., Legrioui, R., & Hamed, Y. (2022). Vulnerability characterization for multi-carbonate aquifer systems in semiarid climate, case of Algerian–Tunisian transboundary basin. *International Journal of Energy and Water Resources*, *6*(1), 67-80. https://doi.org/10.1007/s42108-021-00142-4

Hamad, A., Hadji, R., Bâali, F., Houda, B., Redhaounia, B., Zighmi, K., & Hamed, Y. (2018). Conceptual model for karstic aquifers by combined analysis of GIS, chemical, thermal, and isotopic tools in Tuniso-Algerian transboundary basin. *Arabian Journal of Geosciences*, *11*(15), 1-16. https://doi.org/10.1007/s12517-018-3773-2

Hamed, Y., Hadji, R., Redhaounia, B., Zighmi, K., Bâali, F., & El Gayar, A. (2018). Climate impact on surface and groundwater in North Africa: a global synthesis of findings and recommendations. Euro-Mediterranean *Journal for Environmental Integration*, *3*(1), 25. https://doi.org/10.1007/s41207-018-0067-8

Hamed, Y., Hadji, R., Ncibi, K., Hamad, A., Ben Saad, A., Melki, A., ... & Mustafa, E. (2022a). Modelling of potential groundwater artificial recharge in the transboundary Algero-Tunisian Basin (Tebessa-Gafsa): The application of stable isotopes and hydroinformatics tools. *Irrigation and Drainage*, *71*(1), 137-156.

Hamed, Y., Khelifi, F., Houda, B., Sâad, A. B., Ncibi, K., Hadji, R., ... & Hamad, A. (2022b). Phosphate mining pollution in southern Tunisia: environmental, epidemiological, and socioeconomic investigation. *Environment, Development and Sustainability*, *25*, 13619-13636. https://doi.org/10.1007/s10668-022-02606-x

Hamed, Y., Redhaounia, B., Ben Sâad, A., Hadji, R., & Zahri, F. (2017). Groundwater inrush caused by the fault reactivation and the climate impact in the mining Gafsa basin (southwestern Tunisia). *Journal of Tethys*, *5*(2), 154-164.

Jaballi, F., Felhi, M., Khelifi, M., Fattah, N., Zayani, K., Abbes, N., Elouadi, B., & Tlili, A. (2019). Mineralogical and geochemical behavior of heated natural carbonate-apatite of the Ypresian series, Maknassy-Mezzouna basin, central Tunisia. *Carbonates and Evaporites*, *34*, 1689–1702. https://doi.org/10.1007/s13146-019-00519-x

Jarvis, I., Burnett, W. C., Nathan, Y., Almbaydin, F. S. M., Attia, A. K. M,, Castro, L. N. , Flicoteaux, R., Hilmy, M. E., Husain V., Qutawnah, A. A., Serjani, A., & Zanin, Y. N. (1994). Phosphorite geochemistry state of the-art and environmental concerns. *Eclogae Geologicae Helvetiae*, *87*, 643-700.

Kallel, A., Ksibi, M., Dhia, H. B., & Khélifi, N. (2017). Recent Advances in Environmental Science from the Euro-Mediterranean and Surrounding Regions Proceedings of Euro-Mediterranean Conference for Environmental Integration (EMCEI-1), Tunisia 2017. In Conference proceedings EMCEI (p. 167).

Kechiched, R., Laouar, R., Bruguier, O., Kocsis, L., Salmi-Laouar, S., Bosch, D., Ameur-Zaimeche, O., Foufou, A., & Larit, H. (2020). Comprehensive REE + Y and sensitive redox trace elements of Algerian phosphorites (Tébessa, eastern Algeria): A geochemical study and depositional environments tracking. *Journal of Geochemical Exploration*, *208*, 106396.

Kerbati, N. R., Gadri, L., Hadji, R., Hamad, A., & Boukelloul, M. L. (2020). Graphical and numerical methods for stability analysis in surrounding rock of underground excavations, example of Boukhadra Iron Mine NE Algeria. *Geotechnical and Geological Engineering*, *38*(3), 2725-2733.

McConnell, D. (1973). Apatite: its crystal chemistry, mineralogy utilization and geologic and biologic occurrences. In: *Applied Mineralogy*, *vol 5*. Vienna, New York: Springer.

Ncibi, K., Hadji, R., Hajji, S., Besser, H., Hajlaoui, H., Hamad, A., Mokadem, N., Ben Saad, A., Hamdi, M., & Hamed, Y. (2021). Spatial variation of groundwater vulnerability to nitrate pollution under excessive fertilization using index overlay method in central Tunisia (Sidi Bouzid basin). *Irrigation and Drainage*, *70*(5), 1209-1226. https://doi.org/10.1002/ird.2599

Nekkoub, A., Baali, F., Hadji, R., & Hamed, Y. (2020). The EPIK multi-attribute method for intrinsic vulnerability assessment of karstic aquifer under semi-arid climatic conditions, case of Cheria Plateau, NE Algeria. *Arabian Journal of Geosciences*, *13*(15), 1-15.

Notholt, A. J. G., Sheldon, R. P., & Davidson, D. F. (2005). *Phosphate Deposits of the World: Volume 2, Phosphate Rock Resources*. Cambridge University Press.

Orabi, O. H., El-Sabbagh, A., Mansour, A. S., Ismail, H., & Taha, S. (2023). Foraminifera study for the characterization of the Campanian/Maastrichtian boundary in Gebel Owaina, Nile Valley, Egypt. *Journal of Umm Al-Qura University Applied Sciences*, *9*, 341–359. https://doi.org/10.1007/s43994-023-00043-8

Rais, K., Kara, M., Gadri, L., Hadji, R., & Khochmen, L. (2017). Original approach for the drilling process optimization in open cast mines: Case study of Kef Essenoun open pit mine Northeast of Algeria. *Mining Science*, *24*, 147-159. https://doi.org/10.5277/msc172409

Sankar, T. K., Ambade, B., Mahato, D. K., Kumar, A., & Jangde, R. (2023). Anthropogenic fine aerosol and black carbon distribution over urban environment. *Journal of Umm Al-Qura University Applied Sciences*, *9*, 471–480. https://doi.org/10.1007/s43994-023-00055-4

Sassi S., (1974). La sédimentation phosphatée au Paléocène dans le Sud et le Centre Ouest de la Tunisie. Thèse Doct. ès-Sci. Univ. Paris-Sud Orsay. France.

Sengul, H., Kadir Ozer, A., & Sahin Gulaboglu, M. (2006). Beneficiation of Mardin-Mazıdağı (Turkey) calcareous

phosphate rock using dilute acetic acid solutions. *Chemical Engineering Journal*, *122*(3), 135-140. https://doi.org/10.1016/j.cej.2006.06.005

Stowasser, W. (1975). *Phosphate rocks*. In: U.S. Bureau of Mines, Bulletin 667.

Taib, H., Hadji, R., Hamed, Y., & et al. (2023). Exploring neotectonic activity in a semiarid basin: A case study of the Ain Zerga watershed. *Journal of Umm Al-Qura University Applied Sciences*. Advance online publication. https://doi.org/10.1007/s43994-023-00072-3

Tamani, F., Hadji, R., Hamad, A., & Hamed, Y. (2019). Integrating remotely sensed and GIS data for the detailed geological mapping in semi-arid regions: case of Youks les Bains Area, Tebessa Province, NE Algeria. *Geotechnical and Geological Engineering*, *37*(4), 2903-2913.

Warr, L. N. (2021) IMA-CNMNC approved mineral symbols. *Mineralogical Magazine*, *85*, 291-320. https://doi.org/10.1180/mgm.2021.43

Yi, H., Balan, E., Gervais, C., Segalen, L., Fayon, F., Roche, D., Person, A., Morin, G., Guillaumet, M., Blanchard, M., Lazzeri, M., & Babonneau, F. (2013). A carbonate-fluoride defect model for carbonate-rich fluorapatite. *American Mineralogist*, *98*, 1066-1069.

Zeqiri, R. R., Riheb, H., Karim, Z., Younes, G., Rania, B., & Aniss, M. (2019). Analysis of safety factor of security plates in the mine "Trepça" Stantërg. *Mining Science*, *26*, 21-36. https://doi.org/10.37190/msc192602

Zerzour, O., Gadri, L., Hadji, R., Mebrouk, F., & Hamed, Y. (2020). Semi-variograms and kriging techniques in iron ore reserve categorization: application at Jebel Wenza deposit. *Arabian Journal of Geosciences, 13*, 820. https://doi.org/10.1007/s12517-020-05858-x

Zerzour, O., Gadri, L., Hadji, R., Mebrouk, F., & Hamed, Y. (2021). Geostatistics-Based Method for Irregular Mineral Resource Estimation, in Ouenza Iron Mine, Northeastern Algeria. *Geotechnical and Geological Engineering*, *39*, 3337-3346. https://doi.org/10.1007/s10706-021-01695-1

Zhang, Y., Li, Z., Dini, S. M., Qin, M., Banakhar, A. S., Li, Z., Yi, L., Memesh, A. M., Shammari, A. M., & Li, G. (2021). Origin and Evolution of the Late Cretaceous Reworked Phosphorite in the Sirhan-Turayf Basin, Northern Saudi Arabia. *Minerals*, *11*(4), 350. https://doi.org/10.3390/min11040350

Zhang, Y., Xie, D., Ni, J., & Zeng, X. (2019). Optimizing phosphate fertilizer application to reduce nutrient loss in a mustard (*Brassica juncea var. tumida*)-maize (*Zea mays* L.) rotation system in Three Gorges Reservoir area. *Soil and Tillage Research*, *190*, 78-85. https://doi.org/10.1016/j.still.2019.03.001

Received: 07 Apr 2023
Accepted: 26 Nov 2023
Handling Editor: Tomasz Bajda